IIETA International Information and Engineering Technology Association
Advancing the World of Information and Engineering

Annales de Chimie - Science des Matériaux
Vol. 48, No. 1, February, 2024, pp. 43-55
Journal homepage: http://iieta.org/journals/acsm

Preparation and Characterization of TiO_2-CaO-ZrO_2/HDPE Hybrid Bio-Nanocomposites for Use in Orthopedic Applications

Noor A. Al-Mohammedawi[1*], Shihab A. Zaidan[2], Jenan S. Kashan[1]

[1] Department of Biomedical Engineering, University of Technology, Baghdad 10069, Iraq
[2] Department of Applied Sciences, University of Technology, Baghdad 10069, Iraq

Corresponding Author Email: noor.a.naat@uotechnology.edu.iq

https://doi.org/10.18280/acsm.480106

Received: 2 November 2023
Revised: 25 January 2024
Accepted: 8 February 2024
Available online: 26 February 2024

Keywords:
bone substitute materials, hot-pressing technique, HDPE, TiO_2, CaO-PSZ, FTIR, AFM, DSC

ABSTRACT

In the domain of bone tissue engineering, the quest for suitable bone replacement materials that circumvent the limitations of metallic orthopedic implants is of paramount importance. Metallic implants, despite their wide application and success in orthopedic surgery, are often compromised by inadequate osteoconductive properties and risks of surface corrosion and infection, which can lead to tissue damage and fractures with consequent residual distortion. This study introduces novel bio-nano composite scaffolds fabricated utilizing nanosized fillers—8 mol% CaO-PSZ (partially stabilized zirconia) and TiO_2 (titanium dioxide)—embedded within an HDPE (high-density polyethylene) matrix for potential orthopedic applications. The bio-nano composites were formed under varying compression pressures (29, 114 MPa) and a constant temperature of 150°C for a duration of 15 minutes, resulting in disk-shaped specimens with a diameter of 14.7 mm and heights ranging from 7 to 10 mm. The aim was to determine the optimal thermal and physical properties of these hybrid composites (TiO_2-CaO-PSZ/HDPE) for their use as bone substitutes. Characterization of the scaffolds was conducted via three distinct imaging modalities: Fourier transform infrared spectroscopy (FTIR) for chemical structure elucidation, atomic force microscopy (AFM) for topographical analysis, and differential scanning calorimetry (DSC) for thermal property assessment. The analysis confirmed that the incorporation of nanoparticle fillers into the HDPE matrix resulted in enhanced structural stability and mechanical interlocking at the atomic level. Furthermore, improvements in thermal behavior and crystallization degree were observed in direct correlation with the applied hot-press pressure and the presence of ceramic fillers.

1. INTRODUCTION

Orthopedic injuries and related diseases are a major public health concern, affecting an estimated 1.71 billion people worldwide [1]. The aging population, obesity, and low physical activity have led to a rise in bone problems, requiring bone repair-medicine research [2, 3]. When bone disease approaches a crucial size defect (>5 cm), it requires therapeutic therapy [3]. Orthopedic damage often requires surgery and the use of permanent, temporary, or biodegradable medical implants containing natural or synthetic biomaterials. Device design, the functional properties of the biomaterials, and bioresponse are a few examples of the factors that affect an intervention's clinical effectiveness. [4] Biomaterials are tested for biocompatibility, safety, and effectiveness for clinical use. The ideal material for replacing bodily tissue is one that is comparable or identical to the original. Advances in composite technology have led to the development of novel composites that resemble human tissues, potentially addressing issues with standard implant materials [5]. Materials used to make bone substitutes include polymers, ceramics, metals, and composites. [6] A surface-oxide layer protects metal implants from substantial corrosion, but mechanical stress may surpass this layer's protective ability, resulting in the discharge of hazardous metallic particles. [7] When they reach the joint space, periprosthetic bone, adjacent soft tissues, and distal tissues [8, 9], they induce aseptic implant loosening [10], severe local tissue responses, and/or systemic toxicity [11, 12]. Some ceramics and polymers have been employed as hard-tissue replacement materials (bone substitutes) for many decades. Several of these materials have gained clinical success owing to their unique properties. Several materials from these two groups may be mixed to create composites, which are used in a variety of medical applications. Where Polymers are the most common of these materials because their capacity can be shaped in the desired pattern [13]. Because of its inexpensive cost, excellent strength, and simplicity of production. High-density polyethylene (HDPE) is a polyolefin that is extensively employed in a variety of applications, including biomedicine, owing to its bioinert properties [14]. However, the lives of polyethylene implants are limited owing to wear issues, and PE discharged into the periprosthetic environment causes osteolysis, which leads to implant loosening [15, 16]. Many

studies have looked at the usage of HDPE as bone substitutes in biological applications such as orthopedic prostheses and substitutes [17, 18]. The research [19] tried to investigate the histological and histomorphological responses of porous HDPE by evaluating the tissues histologically and histomorphologically. There was no sign of an initial inflammatory reaction to HDPE with pores, which revealed appropriate osteoconductive qualities. Moreover, the holes were adequate in size and properly linked, allowing for the growth of new tissue. Ceramics and polymer-matrix composites (PMC) allow for physical property tailoring using various types of fillers [20], and TiO_2 nanoparticles are inert, non-toxic, and inexpensive, with inherent self-cleaning mechanisms [21], and are widely used in orthopedics and dentistry, as it is a well-known antibacterial and bone-repairing material with high fracture resistance, ductility, weight-to-strength ratio [22], corrosion resistance [23], and chemical stability [24]. Polymer-based TiO_2-composites of various types have been investigated in the literature, including polyamide/nano-TiO_2 and high-impact polystyrene (HIPS)/nano-TiO_2-composites [25]. Zirconia is a polymorphic structure with three crystal forms: monoclinic (M), cubic (C), and tetragonal (T). Adding oxides like CaO, MgO, and Y_2O_3 (Yttrium) to pure zirconia was shown to make the C-phase more stable. This created a multiphase material called partly stabilized zirconia (PSZ) [26]. Zirconia is a bioceramic substance. They have been employed for bone repair because of various benefits, including nontoxicity and great biocompatibility [27]. Also used as artificial bone fillers to treat bone defects, orthopedic implants, thin films and coatings on various metallic implants, porous bone scaffolds and alternative materials, and bone cements. [28], owing to their superior chemical and electrical resistance, refractory characteristics, thermal stability, corrosion and wear resistance, low friction, high mechanical strength, and relatively high thermal expansion coefficients [28-30]. Kohal et al. [31-33] In three rat femur studies conducted in 2009, 2013, and 2016, zirconia was compared against titanium. In 2009, they concluded that all tested zirconia and titanium implant surfaces were biocompatible and osseoconductive and that the proposed surface modification of zirconia implants produced no difference in histological or biomechanical results when compared to an established electrochemically modified titanium implant surface [31].

A hot-pressing method is used in this study to lessen the effects of thermal deformations and the highest tensile residual stresses that are made normal to the fracture axes when standard polymer fabrication methods are used. This article's main goal is to investigate what happens to nanocomposite polymer matrix systems (TiO_2-CaO-PSZ/HDPE) when different amounts of titanium dioxide and partially stabilized zirconia (PSZ) nanoceramic fillers are added along with a range of compression pressures and reaction temperatures. The thermal properties of these systems are also changed. The goal is to make bioactive biomaterials that can be used for bone repair. Nonisothermal differential scanning calorimetry (DSC) investigations were utilized to investigate the thermal transition parameters of HDPE matrices with low-melting-point (130°C) material and high-melting-point nanoceramic fillers. The surface morphology of the samples was looked at with an atomic force microscope (AFM), and the surface roughness and its effect were measured with an atomic force meter to get bone substitutes and were studied in more detail.

2. EXPERIMENTAL

2.1 Materials

The pure materials (High-density polyethylene, Zirconium Oxide (ZrO_2) stabilized with 8mol% Calcia), Titanium Dioxide) that are used to produce the hybrid nanobiocomposite, as shown in Figure 1. Powder with particle size of (5 µm) and real density of (0.941-0.959 g/cm^3) supplied by Right Fortune Industrial Limited (Shanghai, China) was used as a matrix for the composite material. Zirconium Oxide (ZrO_2) stabilized with 8mol% Calcia powder with average particle size of 40 nm and real density of (6.0-6.1 g/cm^3) supplied by M K Impex Corp. (Canada) was used filler. Titanium Dioxide (TiO_2) powder with average particle size of 50 nm and real density of (3,9 g/ml) supplied by M K Impex Corp. (Canada) was used filler in this study.

2.2 Hybrid bio-nano composites synthesis method

Hybrid-Bio-Nanocomposites were prepared by weighing the composite powders by using precision balances, and then mixed by using roll-ball-milling was used to produce homogenous particles distribution within the composites. The powder components were mixed with three ceramic balls with a diameter range of (2.2 cm). The rotational speed of roll ball milling was set at (11.09 Hz), which equals approximately (665 rpm). The mixing time was 2 hours. All specimens prepared using this mixing time. and then, using the method of the hot-pressing-technique in this technique, the pressure and temperature with each other are applied to the powder mould for preparing the composite specimens. Heating is executed externally using external heaters, and the pressure is applied hydraulically by using (Instron 1195 Series Tension and Compression Tester). To obtain a variety of values during the manufacture of the specimens and cover all manufacturing conditions, two pressures were chosen to produce the specimens (29, 114 MPa) for each composite system. Therefore, the total sum of specimens was (18), as shown in Table 1. For each specimen, sets were fabricated under the same conditions: the temperature degree, duration of heating, and velocity of compression. The specimens were hot-pressed under controlled temperature at (150°C) during (15 min) at velocity (0.5 mm/min) followed by removing the pressure gradually until the specimen cools down and takes the eventual form. The composite specimen's final structure has a disk-shaped diameter of (14.7) mm and (7-10) mm in high. These steps are summarized in a chart, as shown in Figures 1 and 2.

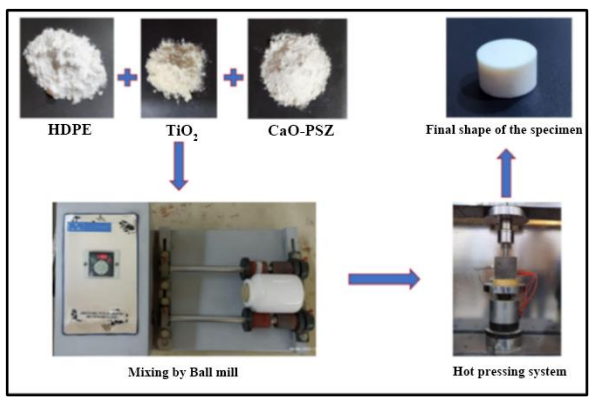

Figure 1. Production of hybrid bio-nanocomposites

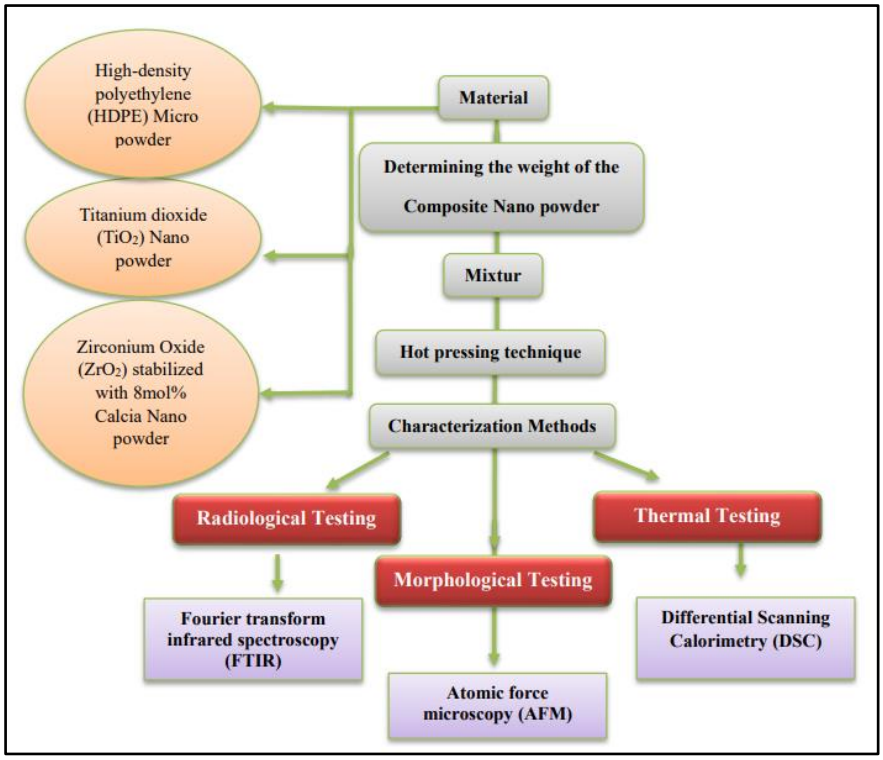

Figure 2. Flow chart of experimental work

Table 1. The selected composition of specimens prepared in this study

Specimens' Composition (wt. %)	Compression Pressure (MPa)
90%HDPE - 5%TiO_2 - 5%CaO-PSZ	29 114
85%HDPE -5%TiO_2 - 10%CaO-PSZ	29 114
80%HDPE -5%TiO_2 - 15%CaO-PSZ	29 114
80%HDPE -10%TiO_2 - 5%CaO-PSZ	29 114
80%HDPE -10%TiO_2 - 10%CaO-PSZ	29 114
80%HDPE -10%TiO_2 - 15%CaO-PSZ	29 114
80%HDPE -15%TiO_2 - 5%CaO-PSZ	29 114
75%HDPE -15%TiO_2 - 10%CaO-PSZ	29 114
70%HDPE -15%TiO_2 - 15%CaO-PSZ	29 114

2.3 Materials characterization techniques

2.3.1 Fourier transform infrared spectroscopy (FTIR)

Fourier-transform infrared spectroscopy is a commonly used method for identifying functional groups in materials (solid, liquid, or gas) using an infrared beam. Fourier-transform infrared (FTIR) spectra were obtained with a resolution of 0,5 cm^{-1} across the range 4000-500 cm^{-1}. Samples were analyzed immediately, with no need to perform any procedures normally used in powder-specimens.

2.3.2 Surface morphology

The morphological evaluations of hybrid bio-nanocomposites (TiO_2-CaO-PSZ/HDPE) samples were conducted using an atomic force microscope (AFM) (Ntegra NT-MDT, Russia) to investigate surface topography (surface roughness and particle size). The tapping method was utilized to administer the examinations.

2.3.3 Differential scanning calorimetry (DSC)

A heat-flux-plate with a thermopile and thermocouples monitoring the heat flow to the reference- and sample-containers are features of an isolated container called a DSC-Furnace. The instrument utilized was a differential scanning calorimeter (DSC-60, Shimadzu, Japan). The sample mass (about 5 mg) was placed within aluminum pans and heated to a continuous temperature of (25 to 180℃) at a rate of 5℃ per minute. The sample was then cooled at a rate of 10℃ per minute.

3. RESULTS AND DISCUSSION

3.1 Radiological analysis by Fourier transform infrared spectroscopy (FTIR) results

The FTIR spectrum of HDPE, TiO_2, and ZrO_2 Nano powder and as a composite in different ratios in the frequency range of (4000 to 400 cm^{-1}) in the transmittance mode, are shown in Figure 3. The molecular structure of HDPE's (CH_2-CH_2) n-repeating unit has been investigated using FTIR. All of the basic modes of vibration have their frequencies assigned. Their chemical structure is confirmed by the full vibrational band assignment provided for both source and commercial HDPE. The FTIR spectrum of HDPE showed the strong asymmetrical (CH_2) stretching aromatic vibrations of the methylene group present in the polymeric sample observed at 2848 cm^{-1} [34]. The appearance of the band in the region of (1736.22, 1649.17, 1549.68, and 1515.14 cm^{-1}) corresponds to (C=O) stretching vibrations. The bands occurring around (1549.68 and 1514.14 cm^{-1}) are due to CH_2 wagging and CH_2 twisting vibrations, respectively [35]. The same results were

previously reported in the works of Guermazi and Gugumus [36-38]. FTIR spectra were used to analyze the various functional groups in TiO_2 nanoparticles. Ti-O bending mode and deformative vibration of Ti-OH stretching mode may be observed from (666.73 to 1689.34 cm-^{1}) respectively. Only the strong peaks lie between (4000 to 500 cm^{-1}) which has been attributed to form TiO_2 nanoparticles the band at (1689.34 cm^{-1}) may be attributed to water adsorbed on the TiO_2 surface [39, 40]. The FTIR-spectrum clearly indicates that the finished product contains Ti-O-Bonds and lacks OH- and Peroxo-Groups [41]. The FTIR spectra of ZrO_2 nanocrystals were recorded in the range of (300-4000 cm^{-1}). The dominant absorption band centered at (446 cm^{-1}) is due to the deformation mode of the Zr-O-Zr bond [42]. The peaks centered at (1130 cm^{-1}) and (1380 cm^{-1}) can be associated with stretching vibrations of Zr-O terminal groups (O- meaning non-bridging atom) [43]. The weak band centered at (1591 cm^{-1}) is assigned to the symmetric bending of H_2O [44] and the band at (2350 cm^{-1}) is due to stretching vibrations of C-O in adsorbed CO_2 from the atmosphere. The wide band centered at (3410 cm^{-1}) is ascribed to the stretching of the O-H group of water [45]. It is evident from (TiO_2-CaO-PSZ/HDPE) that every sample exhibits every chemical group found in pure HDPE, TiO_2, and CaO-PSZ. Peak locations do not slightly change when the compression pressure is increased for samples with the same composition. This explains the strong mechanical interlocking between atoms.

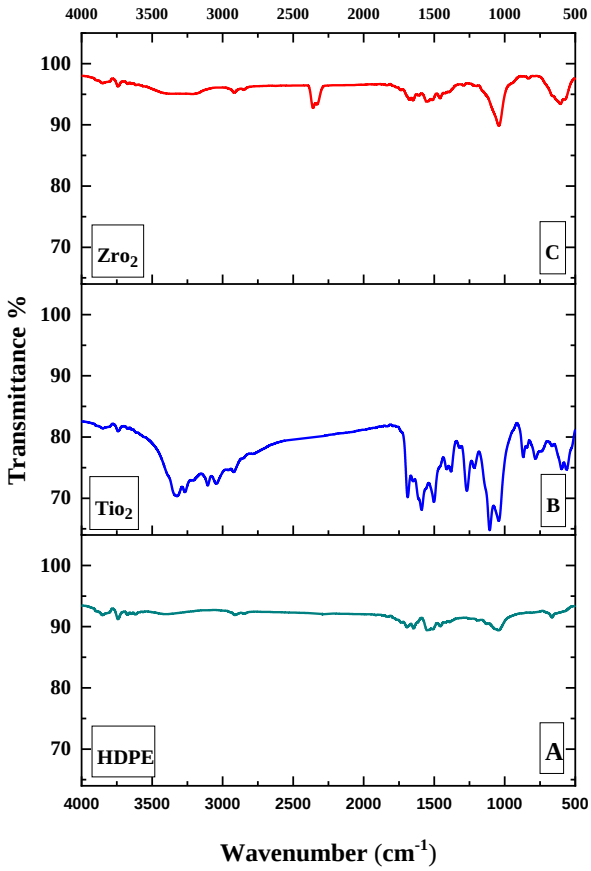

(a) FTIR spectrum results for (HDPE, TiO_2, CaO-PSZ) pure powder

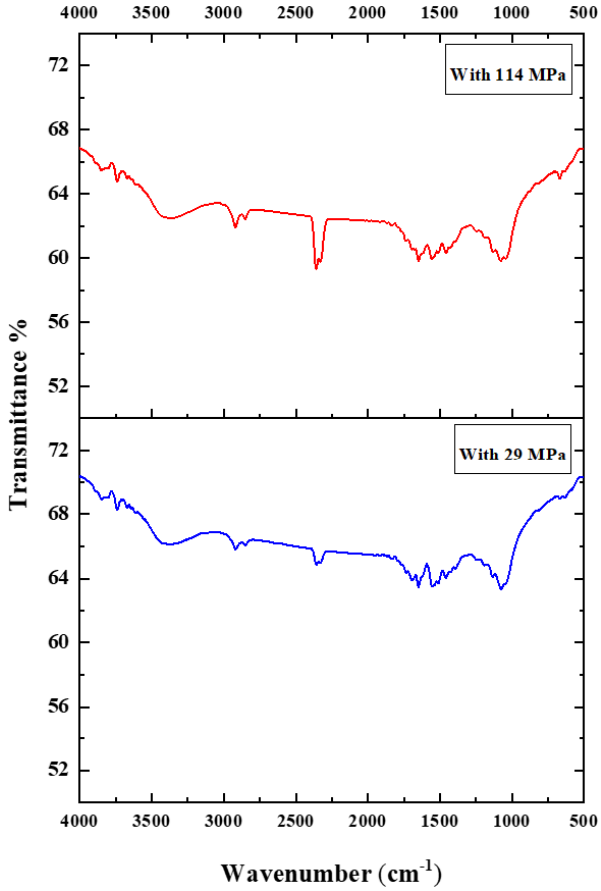

(b) 90%HDPE-5%TiO_2 -5%CaO-PSZ

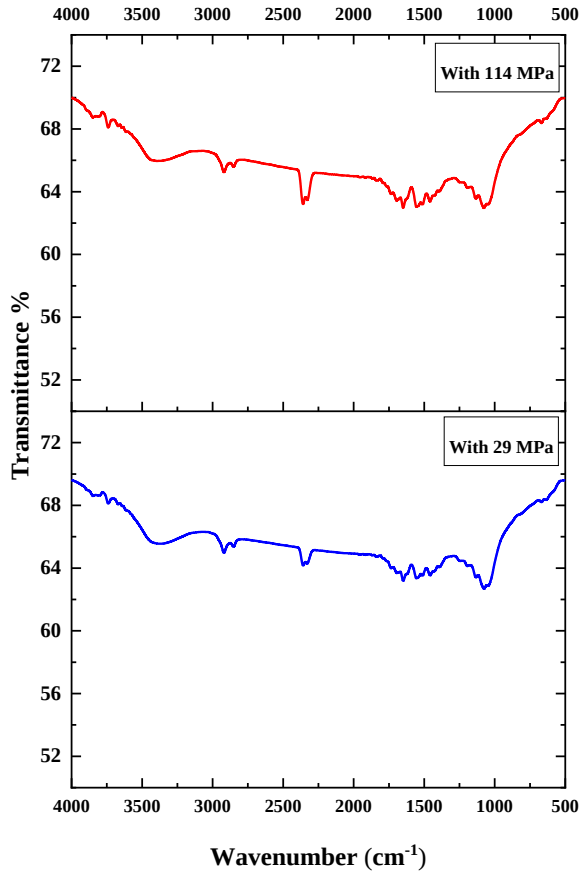

(c) 85%HDPE - 5%TiO_2 - 10%CaO-PSZ

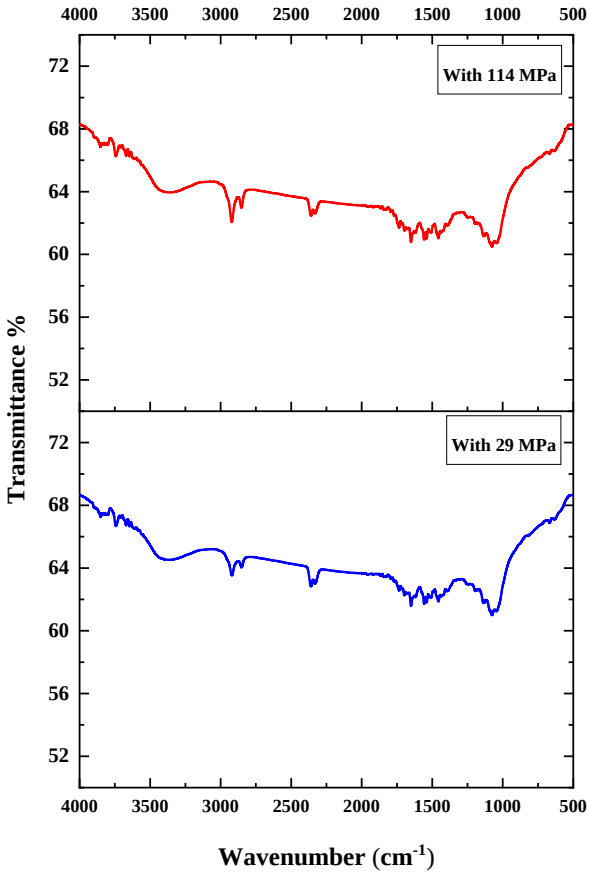

(d) 85%HDPE-10%TiO_2- 5%CaO-PSZ

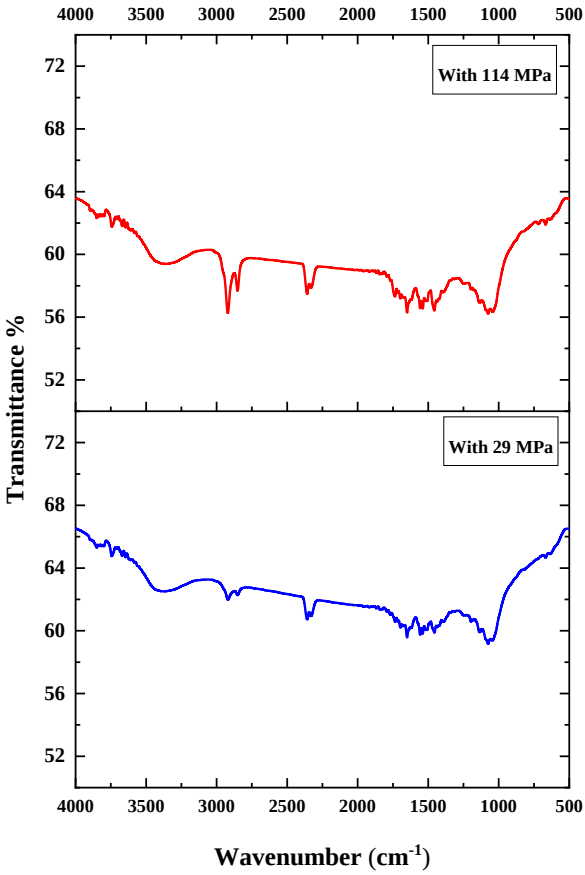

(f) 80%HDPE -10%TiO_2 -10%CaO-PSZ

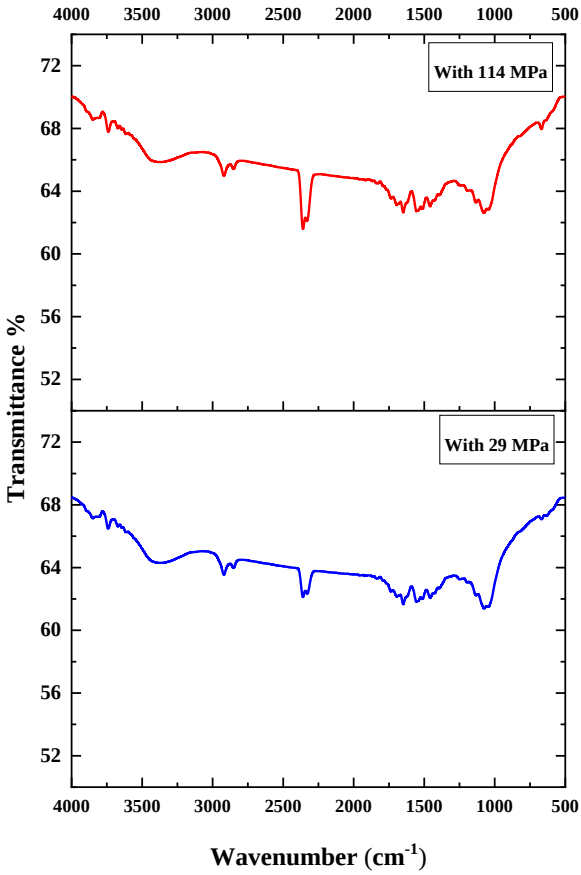

(e) 80%HDPE-5%TiO_2- 15%CaO-PSZ

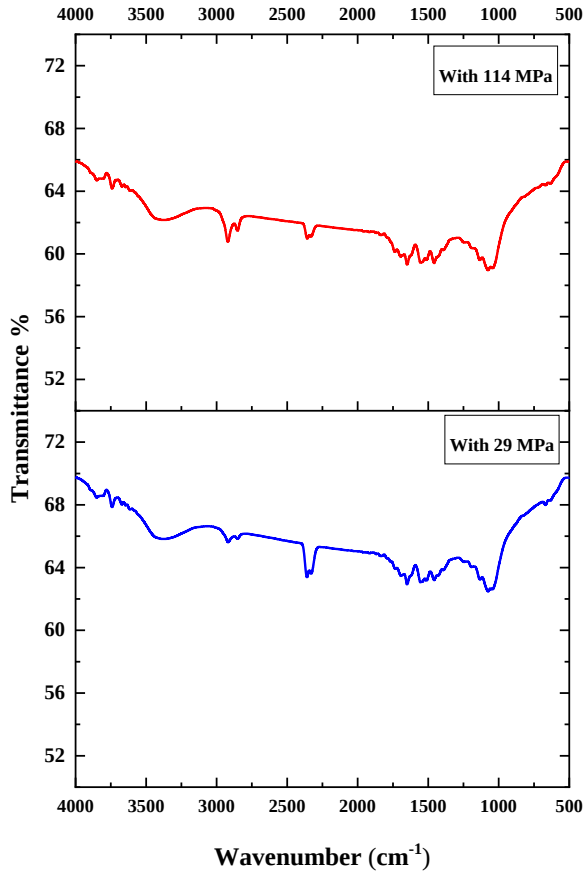

(g) 80%HDPE -15%TiO_2 - 5%CaO-PSZ

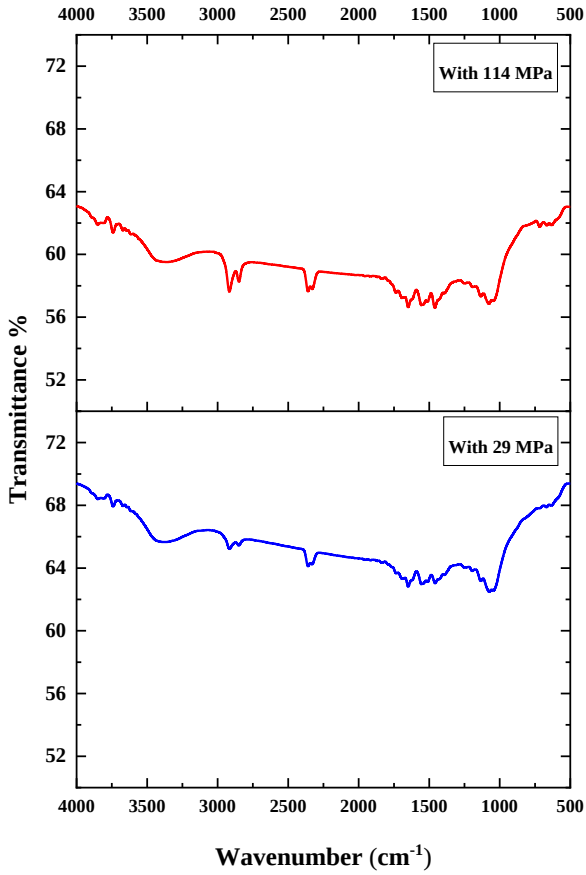

(h) 75%HDPE-15%TiO_2-10%CaO-PSZ

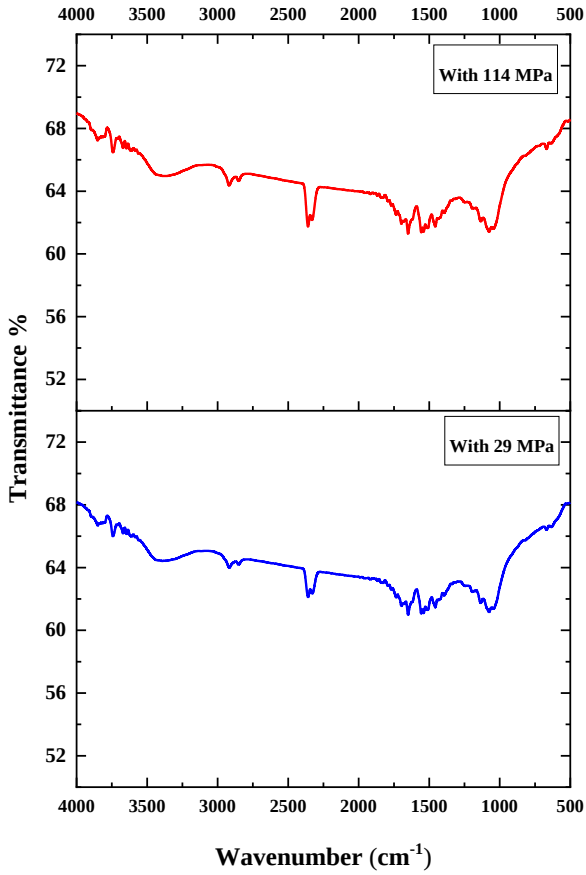

(i) 75%HDPE -10%TiO_2 -15%CaO-PSZ

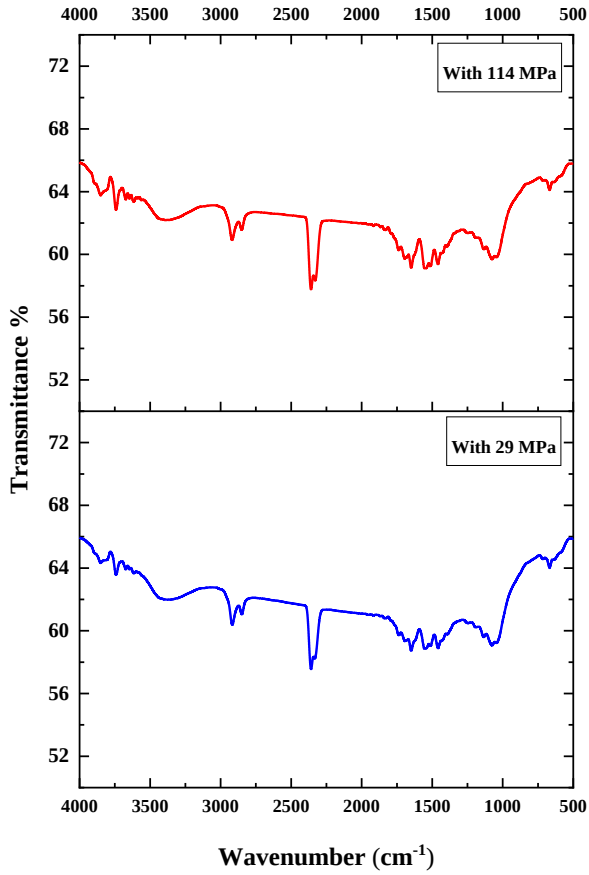

(j) 70%HDPE - 15%TiO_2 - 15%CaO-PSZ

Figure 3. FTIR spectrum results for (TiO_2-CaO-PSZ/HDPE) hybrid bio-nanocomposites with different hot-press pressure (29, 114) Mpa

3.2 Morphological analysis by Atomic Force Microscopy (AFM)

An AFM was performed to study the surface topography of the specimen. It gives a 3-dimensional image of the surface of nanoparticles at an atomic level. and show the effect of hot-press-pressure-difference during specimen-fabrication on the specimen's surface topography and differences in the roughness of the specimen's surface. In Figures 4 and 5 shows 3-D images for the surface roughness examination of (TiO_2-CaO-PSZ/HDPE) Bio-nanocomposites and their grainsize distributions at different Hot-Press-Pressure (29,114) MPa. The values of roughness were listed in Table 2. Atomic force microscopy was used to evaluate the root mean square (RMS) and surface roughness. The data were statistically analyzed to determine the significance of the findings. Furthermore, the specimens' surfaces have undergone fractal analysis. Based on AFM-Topography-Pictures, the surface Roughness of each Specimen has been calculated as the root mean square (RMS) value Rq of the height distribution [46]. Additionally, the Histogram Chart, which showed a uniform normal distribution, demonstrated the consistency of the grain-like characteristics throughout the specimens' surfaces. Grain-size-Distribution-Histogram also shows that the surface of the feature is uniformly distributed shows that the surface of the feature is uniformly distributed across a larger range. Nevertheless, we have a smaller grainsize dispersion and a more uniform, smoother surface topography. Table 2 displays the maximum

particle size, Rq and Ra roughness of 41.05 nm, 5.33 nm, and 3.54 nm for the specimen at 114 MPa hot-press pressure, and the lowest grain size, Rq and Ra of 4.21 nm, 0.96 nm, and 0.74 nm for the specimen at 29 MPa hot-press pressure. Greater hot-press pressure causes greater surface roughness and larger grain sizes, which are indicators of the impact of increasing hot-press pressure on grain-height-uniformity on the surface. The increase in differentiation and cell proliferation is significantly influenced by the roughness of the sample surface [47]. Also, these results demonstrate, that the good homogenous distribution within the polymeric matrix, which explained the subsequent improvement in mechanical characteristics, caused the values of surface roughness to decrease with increases in the % content of fillers (CaO-PSZ and TiO_2). as it will demonstrate. Because there are more grains per unit area, there is a reduction in the surface area of the specimens. Other parameters were also impacted by grain size, particularly mechanical qualities and fracture toughness, which is the most significant [48].

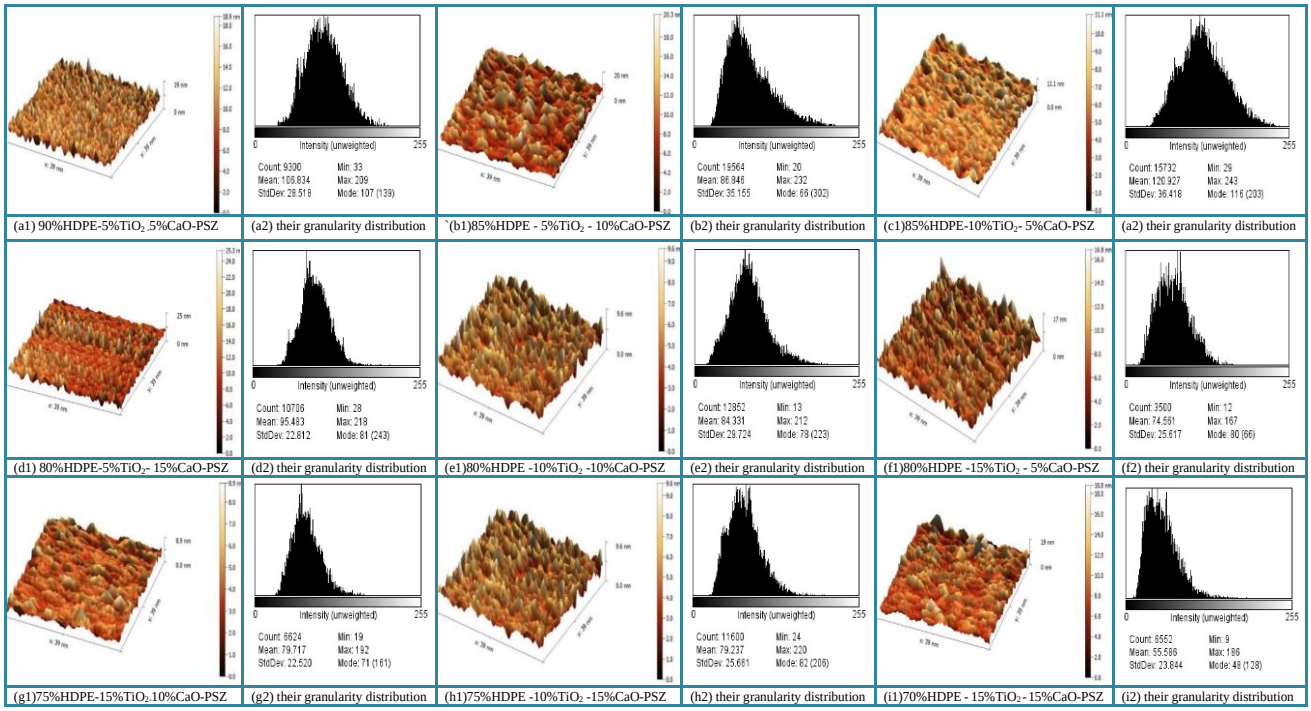

Figure 4. AFM 3D images and their granularity accumulation distribution for (TiO_2-CaO-PSZ/HDPE) hybrid bio-nano composites at hot-press pressure (29) MPa

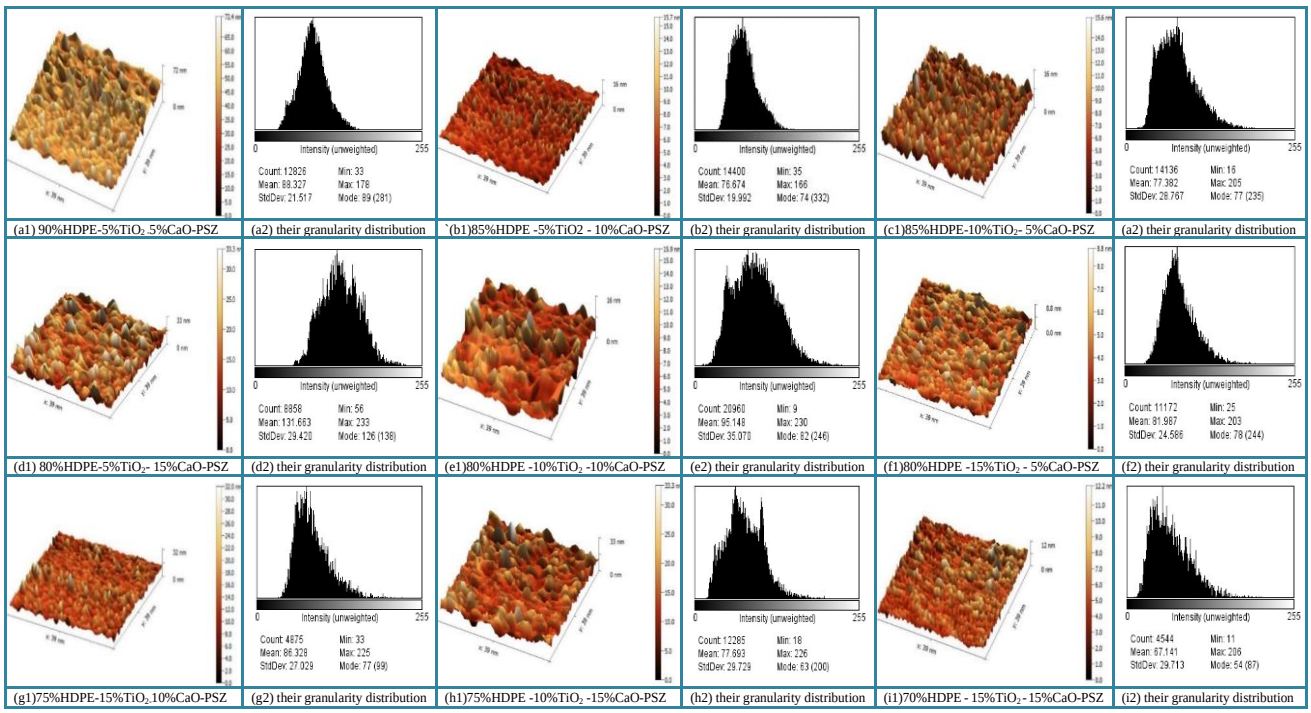

Figure 5. AFM 3D images and their granularity accumulation distribution for (TiO_2-CaO-PSZ/HDPE) hybrid bio-nanocomposites at hot-press pressure (114) MPa

Table 2. AFM parameters with different compositions, for (TiO_2-CaO-PSZ/HDPE) hybrid bio-nanocomposites at different hot-press pressures (29, 114) Mpa

Specimens' Composition (wt. %)	Compression Pressure (MPa)	Avg. Grain Size Diameter (nm)	R_a Roughness Average (nm)	RMS Roughness (nm)
90%HDPE - 5%TiO_2 -	29	9.25	1.97	2.49
5%CaO-PSZ	114	16.97	2.55	3.32
85%HDPE -5%TiO_2 -	29	8.61	1.67	2.20
10%CaO-PSZ	114	11.82	1.67	2.23
80%HDPE -5%TiO_2 -	29	6.54	1.04	1.34
15%CaO-PSZ	114	7.42	1.52	1.93
80%HDPE -10%TiO_2 -	29	17.69	2.18	2.92
5%CaO-PSZ	114	41.05	3.54	5.33
80%HDPE -10%TiO_2 -	29	6.45	1.00	1.27
10%CaO-PSZ	114	8.77	1.68	2.19
80%HDPE -10%TiO_2 -	29	8.71	1.50	1.93
15%CaO-PSZ	114	7.04	0.85	1.10
80%HDPE -15%TiO_2 -	29	4.21	0.74	0.96
5%CaO-PSZ	114	16.38	3.24	4.17
75%HDPE -15%TiO_2 -	29	5.13	0.89	1.12
10%CaO-PSZ	114	13.59	2.39	3.22
70%HDPE -15%TiO_2 -	29	7.47	1.40	1.84
15%CaO-PSZ	114	6.78	1.16	1.50

Table 3. The summary of thermal data for the DSC curves properties with various percentages (wt.%) of (TiO_2-CaO-PSZ/HDPE) hybrid bio-nanocomposites. T_m: The topmost temperature of melting, T_o: The temperature of onset, T_e: Te temperature of endset, ΔH_m: The enthalpy of melting, T_c: The topmost temperature of crystallization, ΔHc: The enthalpy of crystallization, and Xc: The crystallinity degree

Specimen Group	Hot-Press Pressure (MPa)	Melting Stage (°C)			ΔH_m (J/g)	Cooling Stage (°C)			ΔH_c (J/g)	X_C (%)
		(T_m)	(T_o)	(T_e)		(T_c)	(T_o)	(T_e)		
90%HDPE - 5%TiO_2 - 5%CaO-PSZ	29	131	126	133	90	117	115	119	68	31
	114	134	130	136	149	117	114	120	149	51
85%HDPE - 5%TiO_2 - 10%CaO-PSZ	29	132	126	135	268	118	116	121	176	92
	114	132	126	135	224	118	115	120	155	77
85%HDPE -10%TiO_2 - 5%CaO-PSZ	29	132	127	135	164	117	114	120	119	57
	114	134	126	137	184	118	113	120	153	63
80%HDPE -5%TiO_2 - 15%CaO-PSZ	29	133	127	136	162	117	114	120	125	56
	114	132	127	134	193	118	116	121	128	68
80%HDPE -10%TiO_2 -10%CaO-PSZ	29	133	127	137	155	118	114	121	137	53
	114	133	126	135	198	118	114	120	129	68
80%HDPE -15%TiO_2 - 5%CaO-PSZ	29	133	130	136	173	118	113	122	132	60
	114	132	126	135	135	118	115	121	101	47
75%HDPE -15%TiO_2 -10%CaO-PSZ	29	131	125	133	154	119	115	121	98	53
	114	134	129	137	162	118	114	121	114	56
75%HDPE -10%TiO_2 -15%CaO-PSZ	29	133	126	135	165	118	115	121	105	57
	114	132	126	134	155	119	115	121	117	53
70%HDPE -15%TiO_2-15%CaO-PSZ	29	133	126	137	157	118	112	122	136	54
	114	133	126	136	156	118	113	121	121	54

3.3 Thermal analysis by DSC

Thermal stability parameters have been investigated of fabricated nanocomposites systems through measured and calculated data from the area under the curves of temperature's melting and crystallization enthalpies (ΔHm and ΔHc), respectively based on onset of melting (To), melting peak temperature (Tm), Endset temperature (Te), and crystallization peak temperature (Tc) values as obtained from different heating and cooling conditions by differential scanning calorimetry (DSC) using a single non-isothermal method. The thermal behavior for the heat and cooling of nanocomposites (TiO_2-CaO-PSZ/HDPE) are summarized in Table 3 and shown in Figure 6. Heat of fusion (ΔH) is computed by integrating the area under the DSC-endothermic peak [49]. The melting temperature, Tm, was taken as the peak temperature of the transition endothermic curve from the second heating scan, while the crystallization temperature, Tc, was taken as the peak temperature of the transition exothermic curve during the cooling scan [50]. Using the experimental heat of fusion (ΔHm) and the published value of 100% crystalline polymer material (ΔH0m m), the crystallinity of the specimen was determined. According to published research, PE's ΔH0m m is 290 J/g. The proportion of crystallinity (Xc) was estimated using the following equation [49, 51]:

$$Xc = \Delta Hm/(\Delta H°m) *100\% \quad (1)$$

where, Xc is the degree of crystallinity, ΔHm is the specific enthalpy of melting, ΔH0m is the specific enthalpy of melting for 100% crystalline PE. In terms of the effect of pressure or filling percentage on crystallization, the results showed an increase in the degree of crystallinity with increasing pressure and increasing filling percentage in nanocomposite systems.

As the degree of crystallinity of a polymer increases, its mechanical characteristics also rise dramatically [52]. The melting point is unaffected or very slightly changed by increasing pressure or filling percentage.

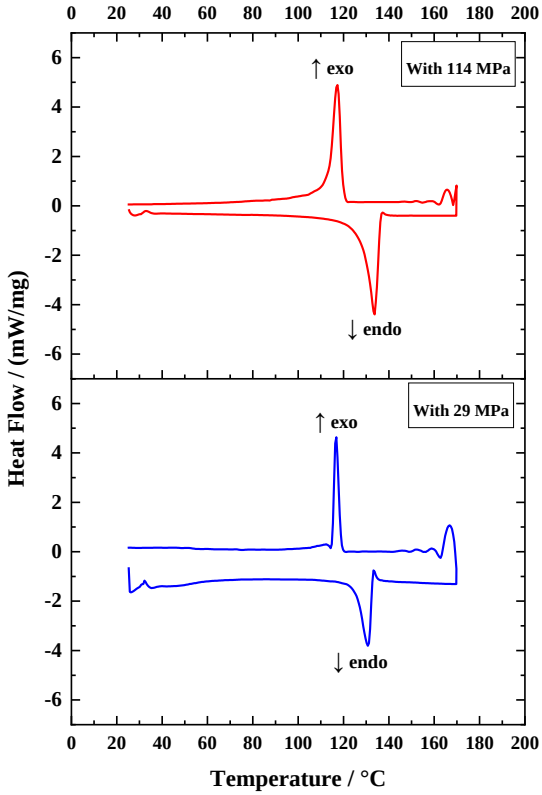

(a) DSC curves for (90%HDPE-5%TiO_2 .5%CaO-PSZ)

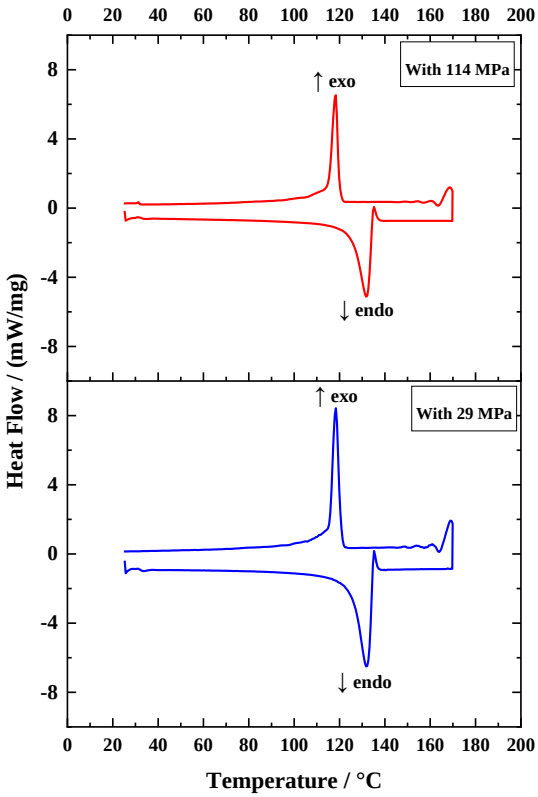

(b) (85%HDPE -5%TiO_2 -10%CaO-PSZ)

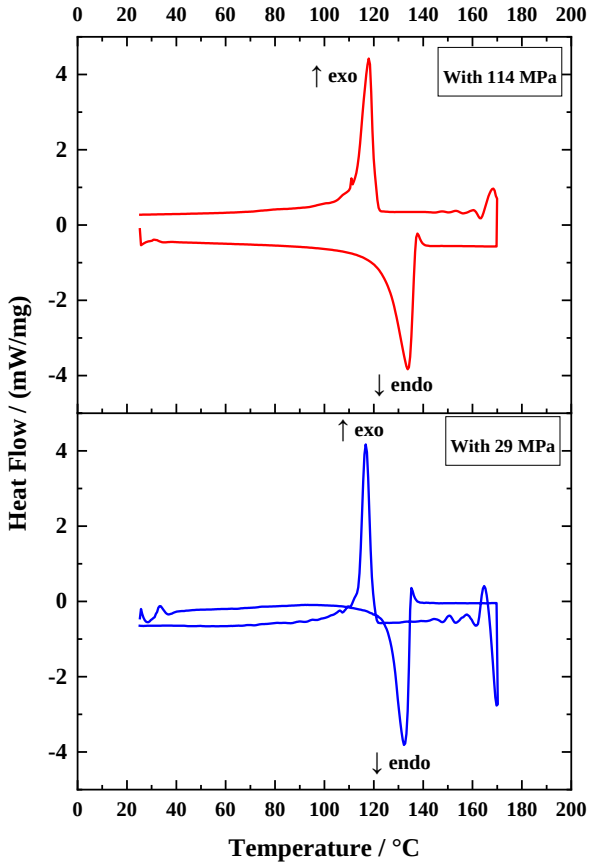

(c) 85%HDPE-10%TiO_2- 5%CaO-PSZ

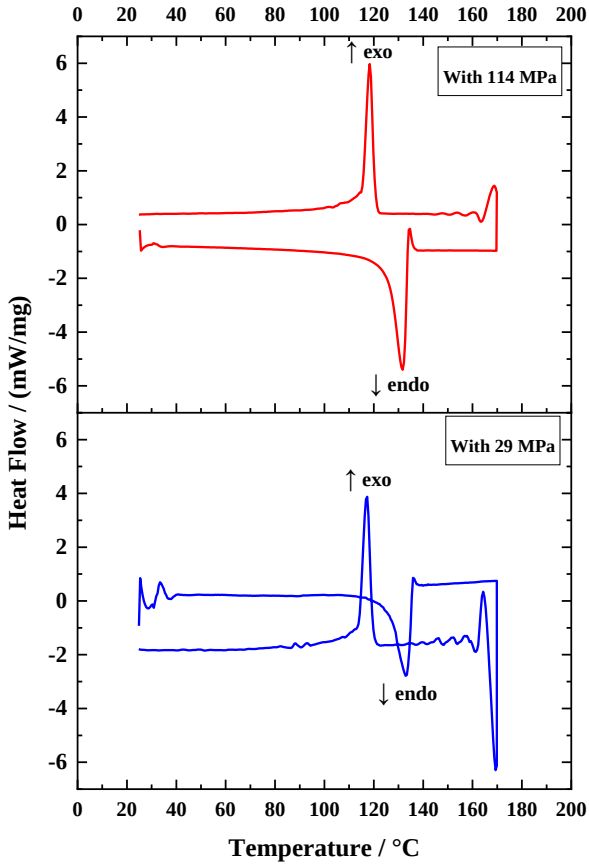

(d) 80%HDPE-5%TiO_2- 15%CaO-PSZ

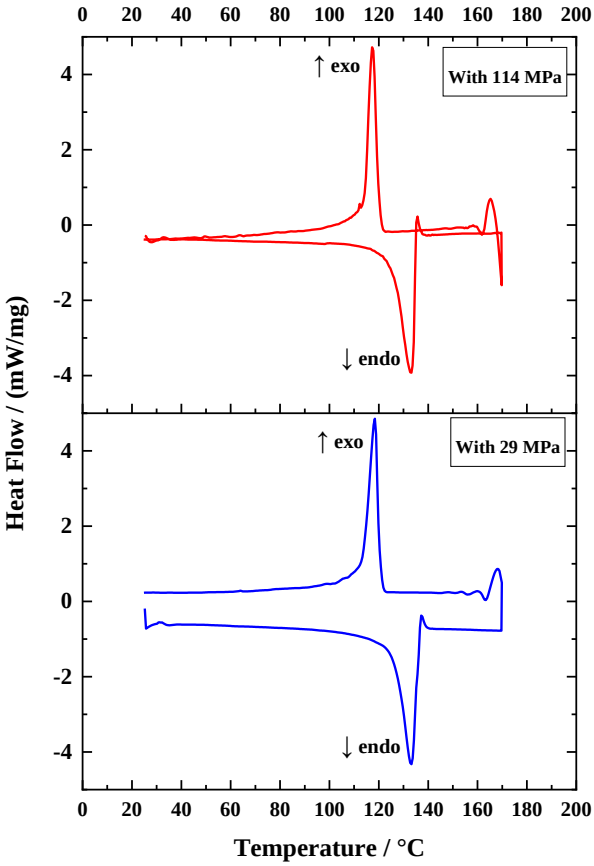

(e) 80%HDPE -10%TiO_2 -10%CaO-PSZ

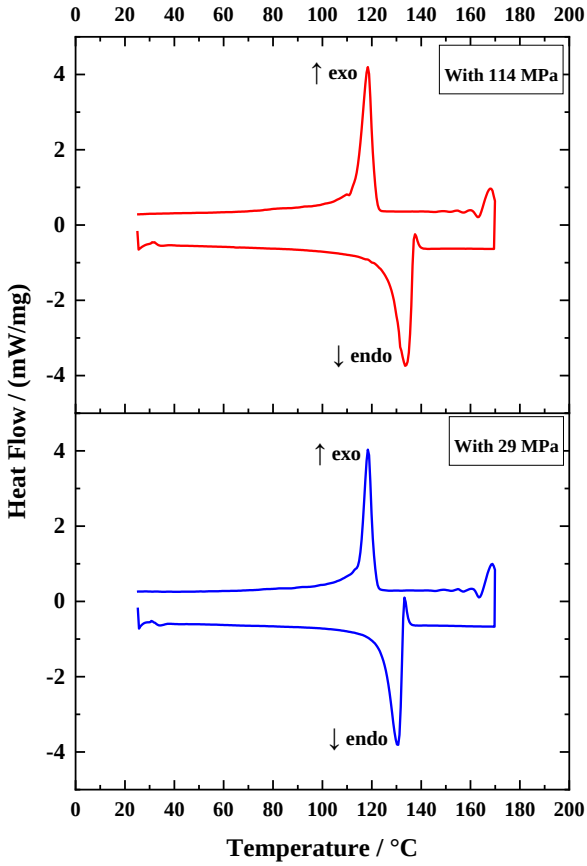

(g)75%HDPE-15%TiO_2-10%CaO-PSZ

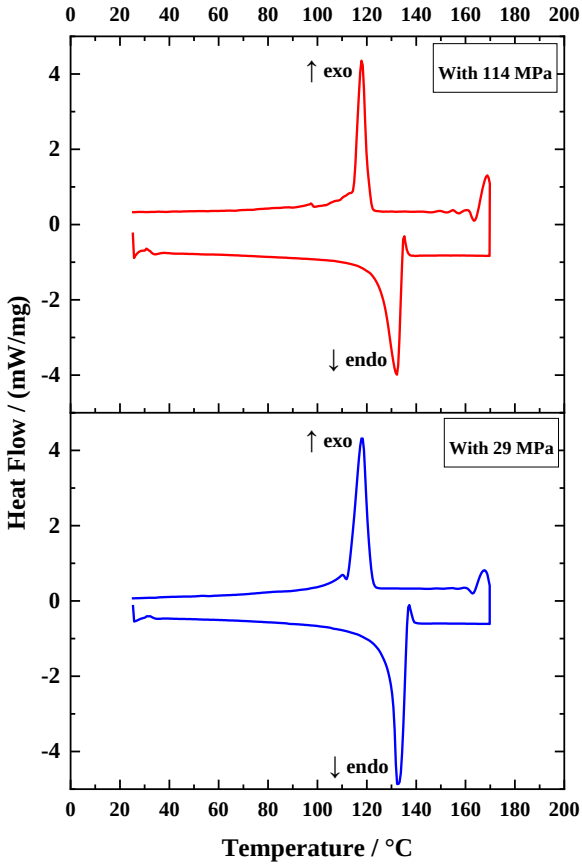

(f) 80%HDPE -15%TiO_2 - 5%CaO-PSZ

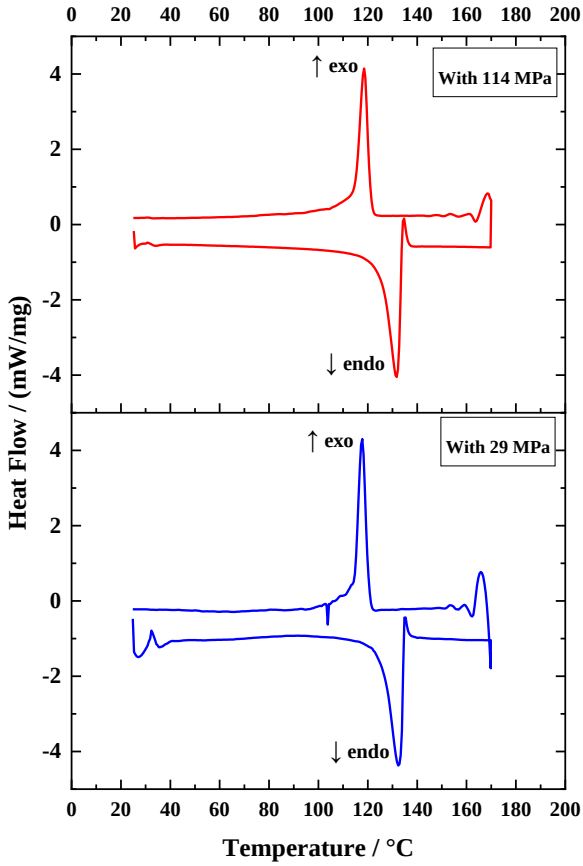

(h) 75%HDPE -10%TiO_2 -15%CaO-PSZ

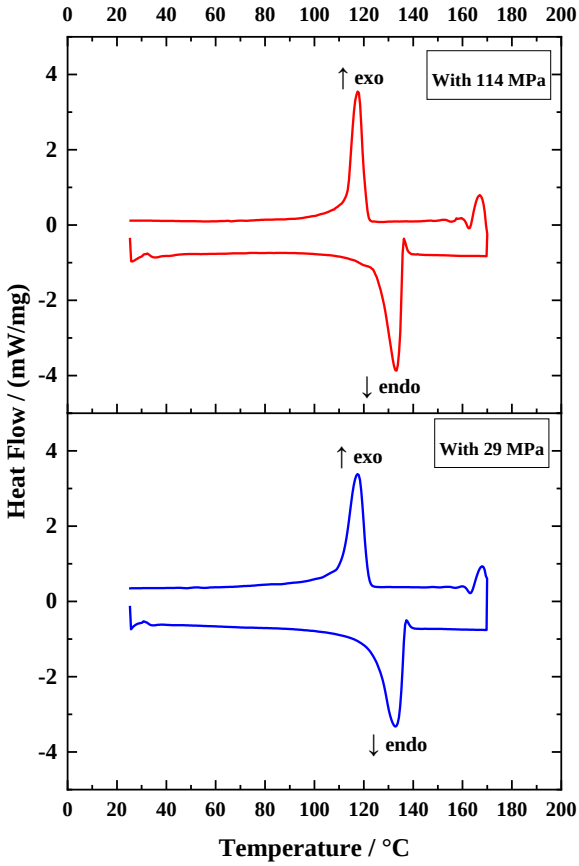

(i) 70%HDPE - 15%TiO_2 - 15%CaO-PSZ

Figure 6. DSC curves for (TiO_2-CaO-PSZ/HDPE)) hybrid bio-nanocomposites recorded with different hot-press pressure (29, 114) MPa

4. CONCLUSIONS

Based on the results displayed in this study, we can conclude the following points:

1- A good texture of the sample has been obtained depending largely on the optimum choice method for mixing ingredients (ball-mill with 2 mixing hours) and sample synthesis method (hot-press technique with 150℃ for 15 min).

2- The FTIR analysis indicated the existence of several bonding types and functional groups in the biocomposite samples. This explains why the composite structure is so stable and adaptable. Increasing compression pressure for the same composition specimens does not cause a slight shift in peak location, explaining the strong mechanical interlocking of atoms.

3- The atomic-force-microscopy (AFM) diagnosis of homogeneous, good microstructure-granularity-distribution for the various nano-composition samples revealed an improvement in the roughness of the specimen surface as well as interconnections between the filler-ceramic-nanoparticles within the polymeric matrices. The sample with the highest surface roughness was composed of 80% HDPE, 5% TiO_2, and 15% CaO-PSZ. The percentage of Roughness increased with increasing the percentage weight of Cao-SPZ compared to TiO_2; Additionally, increasing the hot-press-pressure (from 29 to 114 MPa) increased the roughness, which had an effect on the increase in differentiation and cell proliferation; and surface roughness values decreased with increases in the percentage content of ceramic nanoparticle fillers, due to the excellent nanofiller-particle distribution within polymeric matrices. This provided a nice description of characteristics.

4- Based on a thermal study, the DSC-techniques thermal analysis revealed that in nanocomposite systems there is a rise in the degree of crystallization with pressure and filling percentage. This considerably improves the mechanical characteristics of polymers. Increasing the filling % or the pressure has no effect on the Melting Point, or only slight.

ACKNOWLEDGMENT

Praise be to ALLAH for everything. I am very thankful to everyone who has given me the support I needed to do this work.

REFERENCES

[1] Cieza, A., Causey, K., Kamenov, K., Hanson, S.W., Chatterji, S., Vos, T. (2021). Global estimates of the need for rehabilitation based on the global burden of disease study 2019: A systematic analysis for the global burden of disease study 2019. The Lancet, 396(10267): 2006-2017. https://doi.org/10.1016/S0140-6736(20)32340-0

[2] Ressler, A. (2022). Chitosan-based biomaterials for bone tissue engineering applications: A short review. Polymers, 14(16): 3430. https://doi.org/10.3390/polym14163430

[3] Zhu, G., Zhang, T., Chen, M., Yao, K., Huang, X., Zhang, B., Li, Y., Liu, J., Wang, Y., Zhao, Z. (2021). Bone physiological microenvironment and healing mechanism: Basis for future bone-tissue engineering scaffolds. Bioactive Materials, 6: 4110-4140. https://doi.org/10.1016/j.bioactmat.2021.03.043

[4] Assad, M., Jackson, N. (2019). Biocompatibility evaluation of orthopedic biomaterials and medical devices: A review of safety and efficacy models. Encyclopedia of Biomedical Engineering, 2: 281-309. https://doi.org/10.1016/B978-0-12-801238-3.11104-3

[5] Wang, M. (2004). Bioactive ceramic-polymer composites for tissue replacement. In Engineering Materials for Biomedical Applications, 1-29. https://doi.org/10.1142/9789812562227_0008

[6] Fung, Y.C. (1993). Biomechanics: Mechanical properties of living tissues (2nd ed.). Springer-Verlag. https://doi.org/10.1007/978-1-4757-2257-4

[7] Jacobs, J.J., Gilbert, J.L., Urban, R.M. (1998). Corrosion of metal orthopaedic implants. The Journal of Bone and Joint Surgery. American Volume, 80(2): 268-282. https://doi.org/10.2106/00004623-199802000-00015

[8] Maloney, W.J., Smith, R.L., Schmalzried, T. P., Chiba, J., Huene, D., Rubash, H. (1995). Isolation and characterization of wear particles generated in patients who have had failure of a hip arthroplasty without cement. The Journal of Bone and Joint Surgery. American Volume, 77(9): 1301-1310. https://doi.org/10.2106/00004623-199509000-00002

[9] Urban, R.M., Jacobs, J.J., Tomlinson, M.J., Gavrilovic, J., Black, J., Peoc'h, M. (2000). Dissemination of wear particles to the liver, spleen, and abdominal lymph nodes of patients with hip or knee replacement. The Journal of

Bone & Joint Surgery, 82(4): 457-476. https://doi.org/10.2106/00004623-200004000-00002
[10] Howie, D.W. (1990). Tissue response in relation to type of wear particles around failed hip arthroplasties. The Journal of Arthroplasty, 5(3): 337-348. https://doi.org/10.1016/S0883-5403(08)80093-9
[11] Cooper, H.J., Urban, R.M., Wixson, R.L., Meneghini, R.M., Jacobs, J.J. (2013). Adverse local tissue reaction arising from corrosion at the femoral neck-body junction in a dual-taper stem with a cobalt-chromium modular neck. The Journal of Bone and Joint Surgery. American Volume, 95(10): 865-872. https://doi.org/10.2106/jbjs.l.01042
[12] Bradberry, S.M., Wilkinson, J.M., Ferner, R.E. (2014). Systemic toxicity related to metal hip prostheses. Clinical Toxicology (Philadelphia, Pa.), 52(9): 837-847. https://doi.org/10.3109/15563650.2014.944977
[13] Dhabale, R., Jatti, V.S. (2016). A bio-material: Mechanical behaviour of LDPE-Al2O3-TiO2. In IOP Conference Series: Materials Science and Engineering, Bangalore, India, 149(1): 012043. http://dx.doi.org/10.1088/1757-899X/149/1/012043
[14] Hermán, V., Karam, A., Albano, C., González, G. (2015). High density polyethylene-hydroxyapatite composites synthesized by in situ ethylene polymerization. Revista de la Facultad de Ingeniería Universidad Central de Venezuela, 30(1): 211-218. https://www.researchgate.net/publication/305171888
[15] Jakub, Z., Matsu, R., Martin, V., Jiří, G., Ivan, K., Martin, H. (2018). UHMWPE acetabular cup creep deformation during the run-in phase of THA's life cycle. Journal of the Mechanical Behavior of Biomedical Materials, 87: 30-39. https://doi.org/10.1016/j.jmbbm.2018.07.015
[16] Shahemi, N., Liza, S., Abbas, A., Merican, A.M. (2018). Long-term wear failure analysis of UHMWPE acetabular cup in total hip replacement. Journal of the Mechanical Behavior of Biomedical Materials, 87: 1-9. https://doi.org/10.1016/j.jmbbm.2018.07.017
[17] Balakrishnan, H., Husin, M.R., Wahit, M.U., Abdul Kadir, M.R. (2014). Preparation and characterization of organically modified montmorillonite-filled high density polyethylene/hydroxyapatite nanocomposites for biomedical applications. Polymer-Plastics Technology and Engineering, 53(8): 790-800. http://doi.org/10.1080/03602559.2014.886043
[18] Xu, J., Hu, X., Jiang, S., Wang, Y., Parungao, R., Zheng, S., Nie, Y., Liu, T., Song, K. (2019). The application of multi-walled carbon nanotubes in bone tissue repair hybrid scaffolds and the effect on cell growth in vitro. Polymers, 11(2): 230. https://doi.org/10.3390/polym11020230
[19] Martínez Rodríguez, J., Renou, S.J., Guglielmotti, M.B., Olmedo, D.G. (2019). Tissue response to porous high-density polyethylene as a three-dimensional scaffold for bone tissue engineering: An experimental study. Journal of Biomaterials Science, Polymer Edition, 30(5): 486-499. https://doi.org/10.1080/09205063.2019.1582278
[20] Thomas, H., Dorothée, V.S. (2010). Polymer-Nanoparticle Composites: From Synthesis to Modern Applications. Materials, 3(6): 3468-3517. https://doi.org/10.3390/ma3063468
[21] Daniela, Y., Sichem, G., Ingo, L., María T.U., Tatiana, G., Franco, M.R., Paula, A.Z. (2015). Photocatalytic inhibition of bacteria by TiO_2 nanotubes-doped polyethylene composites. Applied Catalysis A: General, 489: 255-261. https://doi.org/10.1016/j.apcata.2014.10.051
[22] Khaled, S.M., Sui, R., Charpentier, P.A., Rizkalla, A.S. (2007). Langmuir, 23(7): 3988-3995. https://doi.org/10.1021/la063222v
[23] Lai, Y., Cheng, Y., Yang, H., Yang, Y., Huang, J., Chen, Z., Wang, X., Lin, C. (2018). Progress in TiO2 nanotube coatings for biomedical applications: A review. Journal of Materials Chemistry B, 6: 1862-1886. https://doi.org/10.1039/C8TB00149A
[24] Imran, M., Riaz, S., Naseem, S. (2012). Materials Today: Proceedings, 2. Elsevier Ltd. Retrieved from https://www.materialstoday.com/proceedings.
[25] Abdul Kaleel, S.H., Bahuleyan, B.K., Masihullah, J., Al-Harthi, M. (2011). Thermal and Mechanical Properties of Polyethylene/Doped-TiO2 Nanocomposites Synthesized Using in Situ Polymerization. Journal of Nanomaterials, 2011: 1-6. https://doi.org/10.1155/2011/964353
[26] Popescu, S.M., Manolea, H.O., Diaconu, O.A., Mercuț, R., Scrieciu, M., Dascălu, I.T., Țuculină, M.J., Obădan, F., Popescu, F.D. (2017). Zirconia biocompatibility in animal studies-A systematic review. Defect and Diffusion Forum, 376: 12-28. https://doi.org/10.4028/www.scientific.net/DDF.376.12.
[27] Raghavendra, S.S., Jadhav, G.R., Gathani, K.M., Kotadia, P. (2017). Bioceramics in endodontics - a review. Journal of Istanbul University Faculty of Dentistry, 51: S128-S137. https://doi.org/10.17096/jiufd.63659
[28] Afzal, A. (2014). Implantable zirconia bioceramics for bone repair and replacement: A chronological review. Materials Express, 4(1): 1-12. http://doi.org/10.1166/mex.2014.1148
[29] Bartolomé, J.F., Smirnov, A., Kurland, H.D., Grabow, J., Müller, F.A. (2016). New ZrO2/Al2O3 nanocomposite fabricated from hybrid nanoparticles prepared by CO2 laser co-vaporization. Scientific Reports, 6: 20589. https://doi.org/10.1038/srep20589
[30] Thirupathy, M., Dhanapal, B., Suresh, S. (2016). Synthesis and characterization of yttrium stabilized zirconia nanoparticles. Materials Research, 19(4): 812-816. https://doi.org/10.1590/1980-5373-MR-2016-0196
[31] Kohal, R.J., Wolkewitz, M., Hinze, M., Han, J.S., Bächle, M., Butz, F. (2009). Biomechanical and histological behavior of zirconia implants: An experiment in the rat. Clinical Oral Implants Research, 20(4): 333-339. https://doi.org/10.1111/j.1600-0501.2008.01656.x
[32] Kohal, R.J., Bächle, M., Att, W., Chaar, S., Altmann, B., Renz, A., Butz, F. (2013). Osteoblast and bone tissue response to surface modified zirconia and titanium implant materials. Dental Materials, 29(7): 763-776. https://doi.org/10.1016/j.dental.2013.04.003
[33] Kohal, R.J., Bächle, M., Renz, A., Butz, F. (2016). Evaluation of alumina toughened zirconia implants with a sintered, moderately rough surface: An experiment in the rat. Dental Materials, 32(1): 65-72. https://doi.org/10.1016/j.dental.2015.10.008
[34] Socrates, G. (1994). Infrared Characteristic Group Frequencies: Tables & Charts. John Wiley & Sons.
[35] Silverstein, R.M., Bassler, G.C., Morrill, T.C. (1991). Spectroscopic Identification of Organic Compounds. John Wiley & Sons.
[36] Guermazi, N., Elleuch, K., Ayedi, H.F. (2009). The effect of time and aging temperature on structural and

mechanical properties of pipeline coating. Materials and Design, 30(5): 2006-2010. http://doi.org/10.1016/j.matdes.2008.09.003

[37] Gugumus, F. (1998). Critical antioxidant concentrations in polymer oxidation - III: Application to lifetime prediction. Polymer Degradation and Stability, 60(1-3): 119-135. https://doi.org/10.1016/S0141-3910(97)00033-5

[38] Gugumus, F. (1995). The performance of light stabilizers in accelerated and natural weathering. Polymer Degradation and Stability, 50(1): 101-116. https://doi.org/10.1016/0141-3910(95)00134-8

[39] Abazari, R., Mahjoub, A.R., Sanati, S. (2014). A facile and efficient preparation of anatase titania nanoparticles in micelle nanoreactors: Morphology, structure, and their high photocatalytic activity under UV light illumination. RSC Advances, 4: 56406. https://doi.org/10.1039/C4RA10018B

[40] Antic, Z., Krsmanovic, R.M., Nikolic, M.G., Cincovic, M.M., Mitric, M., Polizzi, S., Dramicanin, M. D. (2012). Materials Chemistry and Physics, 135(3): 1064. http://dx.doi.org/10.1016/j.matchemphys.2012.06.016

[41] Rajakumar, G., Rahuman, A.A., Roopan, S.M., Khanna, V.G., Elango, G., Kamaraj, C., Zahir, A.A., Velayutham, K. (2012). Fungus-mediated biosynthesis and characterization of TiO2 nanoparticles and their activity against pathogenic bacteria. Spectrochimica Acta Part A: Molecular and Biomolecular Spectroscopy, 91: 23-29. https://doi.org/10.1016/j.saa.2012.01.011

[42] Niasari, M.S., Dadkhah, M., Davar, F. (2009). Pure cubic ZrO_2 nanoparticles by thermolysis of a new precursor. Journal of Polymer Science, 28(14): 3005-3009. https://doi.org/10.1016/j.poly.2009.06.032

[43] Badenes, J.A., Vicent, J.B., Llusar, M., Tena, M.A., Monros, G. (2002). The nature of Pr-$ZrSiO_4$ yellow ceramic pigment. Journal of Materials Science, 37: 1413-1420. https://doi.org/10.1023/A:1014537000690

[44] Dong, W.-S., Lin, F.-Q., Liu, C.-L., Li, M.-Y. (2009). Synthesis of ZrO_2 nanowires by ionic-liquid route. Journal of Colloid and Interface Science, 333: 734-740. https://doi.org/10.1016/j.jcis.2009.02.025

[45] Prakashbabu, D., Krishna, R.H., Nagabhushana, B.M., Nagabhushana, H., Shivakumara, C., Chakradar, R.P.S., Ramalingam, H.B., Sharma, S.C., Chandramohan, R. (2014). Low temperature synthesis of pure cubic ZrO2 nanopowder: Structural and luminescence studies. Spectrochimica Acta Part A: Molecular and Biomolecular Spectroscopy, 122: 216-222. https://doi.org/10.1016/j.saa.2013.11.043

[46] Salerno, M., Giacomelli, L., Derchi, G., Patra, N., Diaspro, A. (2010). Atomic force microscopy in vitro study of surface roughness and fractal character of a dental restoration composite after air-polishing. BioMedical Engineering OnLine, 9(1): 59. https://doi.org/10.1186/1475-925X-9-59

[47] Liang, C., Luo, Y., Yang, G., Xia, D., Liu, L., Zhang, X., Wang, H. (2018). Graphene oxide hybridized nHAC/PLGA scaffolds facilitate the proliferation of MC3T3-E1 cells. Nanoscale Research Letters, 13(1): 1-10. https://doi.org/10.1186/s11671-018-2432-6

[48] Trunec, M. (2008). Effect of grain size on mechanical properties of 3Y-TZP ceramics. Ceramics-Silikáty, 52: 165-171.

[49] Chafidz, A., Al-haj Ali, M., Elleithy, R. (2011). Morphological, thermal, rheological, and mechanical properties of polypropylene-nanoclay composites prepared from masterbatch in a twin-screw extruder. Journal of Materials Science, 46: 6075-6086. https://doi.org/10.1007/s10853-011-5570-0

[50] Fouad, H., Elleithy, R. (2011). High density polyethylene/graphite nano-composites for total hip joint replacements: Processing and in vitro characterization. Journal of the Mechanical Behavior of Biomedical Materials, 4: 1376. https://doi.org/10.1016/j.jmbbm.2011.05.008

[51] Salkhi Khasraghi, S., Rezaei, M., Razavi, M.K., Aghjeh, M. (2011). Melt crystallization behavior and non-isothermal crystallization kinetics of UHMWPE/HDPE/MWCNTs nanocomposite. In Proceedings of the Polymer Processing Society Asia/Australia Regional Meeting, Kish Island, 15-17.

[52] Dusunceli, N., Colak, O.U. (2008). Modelling effects of degree of crystallinity on mechanical behavior of semicrystalline polymers. International Journal of Plasticity, 24(7): 1224-1242. https://doi.org/10.1016/j.ijplas.2007.09.003